Volume 58
Number 62
11 August 2022
Pages 8591–8724

ChemComm

Chemical Communications

rsc.li/chemcomm

ISSN 1359-7345

ROYAL SOCIETY OF CHEMISTRY

COMMUNICATION

Frédéric Coutrot, Yann Ferrand *et al.*
[3]Foldarotaxane-mediated synthesis of an improbable [2]rotaxane

ChemComm

COMMUNICATION

View Article Online
View Journal | View Issue

Cite this: *Chem. Commun.*, 2022, **58**, 8618

Received 30th May 2022,
Accepted 27th June 2022

DOI: 10.1039/d2cc03066g

rsc.li/chemcomm

[3]Foldarotaxane-mediated synthesis of an improbable [2]rotaxane†

Victor Koehler,‡[a] Maxime Gauthier,‡[b] Chenhao Yao,[a] Karine Fournel-Marotte,[b] Philip Waelès,[b] Brice Kauffmann,[c] Ivan Huc,[d] Frédéric Coutrot *[b] and Yann Ferrand*[a]

The wrapping of an aromatic oligoamide helix around an active ester-containing [2]rotaxane enforced the sliding and the sequestration of the surrounding macrocycle around a part of the axle for which it has no formal affinity. The foldamer-mediated compartmentalization of the [2]rotaxane shuttle was subsequently used to prepare an improbable rotaxane.

Mechanically interlocked molecules such as rotaxanes are appealing compounds for potential applications in fields as varied as materials science[1] and biology.[2] A [2]rotaxane consists of a molecular axle that threads through a macrocycle. Bulky stoppering units at each end of the axle sterically ensure the mechanical bond[3] by preventing the macrocycle from dethreading. The non-covalent assembly allows for co-conformational degrees of freedom of the interlocked elements with respect to one another. Taking advantage of this, numerous well-thought [2]rotaxanes have been reported in the literature with the aim of operating as molecular shuttles,[4] through the controlled translational motion of the surrounding macrocycle between sites of interactions (called molecular stations) on the encircled axle.[5] Most of these co-conformational changes may be triggered by the alteration of the interactions between the macrocycle and its axle thanks to an external stimulus such as a chemical reaction,[6] photo-irradiation,[7] variation in solvent polarity[8] or temperature,[9] or recognition of ions.[10] Much scarcer are the examples relative to the control of the macrocycle localization due to an intermolecular recognition of a neutral compound.[11] Berna has reported a rotaxane with two diacylaminopyridine-stations, which upon binding of barbital to these stations leads to a change in the co-conformational behavior of the macrocycle. Recently, we reported the formation of a foldarotaxane architecture consisting in a [2]rotaxane, the axle of which is also wrapped by a foldamer helix.[12] We showed that the winding of the helix around the encircled axle can be altered by the macrocycle localisation. Here, we investigate the reciprocal effect. We propose the utilization of aromatic oligoamide helix **1** as a supramolecular auxiliary aimed at compartmentalizing [2]rotaxane **3-Boc** through efficient intermolecular binding (Fig. 1). By interfering with the interaction site of the dibenzo-24-crown-8 (DB24C8) macrocycle (*i.e.* the amide site) and by hindering most of the "left" side of the encircled axle with respect to the *N*-hydroxysuccinimide (NHS) ester, the helix was envisaged to displace the DB24C8 away from its preferred amide station and to force it to move on an axle section devoid of any strong site of interaction. Subsequent aminolysis of the NHS ester of foldarotaxane **1⊃3-Boc** may then yield the improbable§,[13] [2]rotaxane **6**, that is, a [2]rotaxane devoid of any formal mutual recognition elements which would enable rotaxane formation (Fig. 1a). Reference [2]rotaxane **3-HPF$_6$** was considered as the precursor of the targeted **3-Boc** (see the ESI† for its synthesis). The encircled axle of **3-HPF$_6$** contained the motifs that were necessary to drive its assembly from both DB24C8 and single helix **1**. First, the ammonium[14] (Fig. 1a top, cyan) served as a template for the synthesis of the DB24C8-based [2]rotaxane *via* a slipping-then-capping strategy. Second, the amide function (Fig. 1a, purple) was chosen to act as a secondary molecular station of lower affinity for the DB24C8 compared to the ammonium,[13b,15] therefore allowing for the shuttling of the macrocycle upon concealing the ammonium station. Noteworthy, complemented by a carbamate group (Fig. 1a and c orange), the amide moiety was also intended to serve as a recognition motif for dissymmetrical helix **1**. The latter was designed specifically with two differentiated ends,

[a] *Institut de Chimie et Biologie des Membranes et Nano-objets CBMN (UMR5248), Université de Bordeaux, CNRS, IPB, 2 rue Robert Escarpit, 33600, Pessac, France. E-mail: y.ferrand@iecb.u-bordeaux.fr*

[b] *Supramolecular Machines and Archtectures Team, IBMM, Univ Montpellier, CNRS, ENSCM, Montpellier, France. E-mail: frederic.coutrot@umontpellier.fr; Web: https://www.glycorotaxane.fr*

[c] *Université de Bordeaux, CNRS, INSERM, UMS3033, IECB, 2 rue Robert Escarpit, 33600, Pessac, France*

[d] *Department of Pharmacy, Ludwig-Maximilians-Universität, Butenandtstr. 5–13, 81377, München, Germany*

† Electronic supplementary information (ESI) available. CCDC 2175298 for **1⊃2**. For ESI and crystallographic data in CIF or other electronic format see DOI: https://doi.org/10.1039/d2cc03066g

‡ These authors contributed equally to this work.

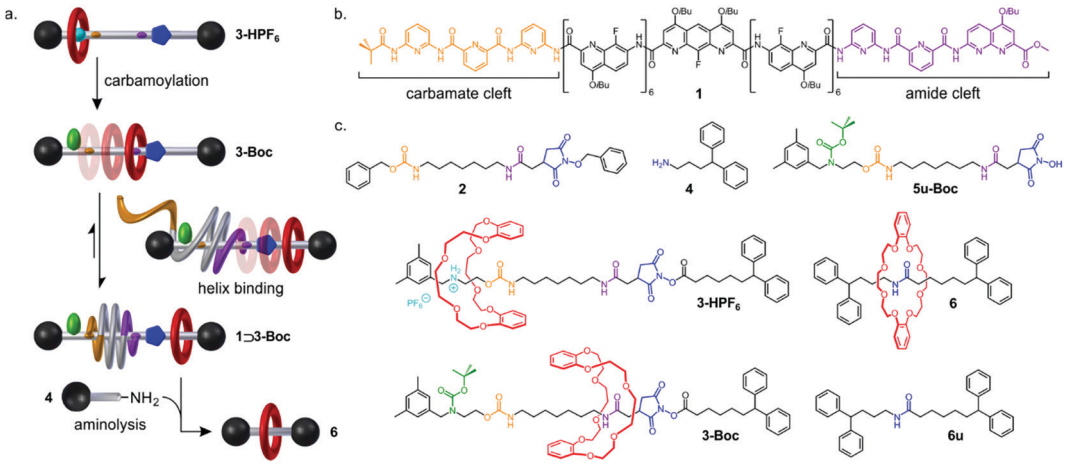

Fig. 1 (a) Schematic representation of the successive molecular machineries, first between the [2]rotaxanes **3-HPF$_6$** and **3-Boc** through deprotonation-then-carbamoylation of the ammonium, then by the displacement and sequestration of the DB24C8 after the entwining of the helix to produce a foldarotaxane. The helix binding induces the displacement of the macrocycle that becomes sequestrated on a part of the axle for which it has no affinity. It follows that the cleavage of the axle can yield a [2]rotaxane. (b) Sequence of the dissymmetrical helix **1** and (c) formulae of rotaxanes **3-HPF$_6$**, **3-Boc** and **6** and non-interlocked molecular axles and reactants **2**, **4**, **5u-Boc** and **6u**.

a carbamate cleft and an amide cleft (Fig. 1b), capable of binding to carbamate and amide moieties spaced by a seven methylene α,ω-alkane chain with high affinity in chloroform ($K_a > 10^5$ M^{-1}).[16] A cleavable NHS ester link was placed between two sections of the encircled axle with the aim of obtaining the shorter [2]rotaxane **6** that is devoid of any formal mutual site of recognition between the DB24C8 and the axle and could not be obtained efficiently by a template-mediated threading-and-capping strategy. In **3-HPF$_6$**, the DB24C8 was mainly localized around the best ammonium station. Deprotonation–carbamoylation of the ammonium caused the gliding of the DB24C8 towards the amide secondary station (see the ESI† for the ^{1}H NMR evidences related to the localization of the DB24C8 along the encircled axle in **3-HPF$_6$** and **3-Boc**). In **3-HPF$_6$** and **3-Boc**, the DB24C8 was thus localized on the "left" side of the axle with respect to the NHS ester. The NHS moiety not being bulky enough to preserve the mechanical bond, cleavage of the rotaxane axle through aminolysis of the active ester would result in the irremediable loss of the interlocked architecture, therefore providing the free macrocycle along with axle fragments. Before envisioning the cleavage of the NHS ester link, we thus considered the possibility to wrap the foldamer helix **1** around the encircled axle of **3-Boc** in order to displace the surrounding DB24C8 around the sole vacant unhindered "right" part of the axle with respect to the NHS.

A preliminary experiment was performed to evaluate the ability of **1** to form a foldaxane[17] by wrapping around the carbamate–amide binding site of model axle **2** despite the close proximity of the *O*-benzyl NHS moiety (Fig. 2). Titration of single helix **1** by **2** was carried out in $CDCl_3$. ^{1}H and ^{19}F NMR monitoring revealed changes consistent with the formation **1⊃2** in slow exchange with the free helix on the NMR time scale (Fig. 2a–d and Fig. S4, S5, ESI†). As expected, mixing the racemic helix **1**, that is, the mixture of *P* and *M* enantiomeric conformers, with racemic axle (R/S)-**2** led to the emergence of two sets of new resonances corresponding to two pairs

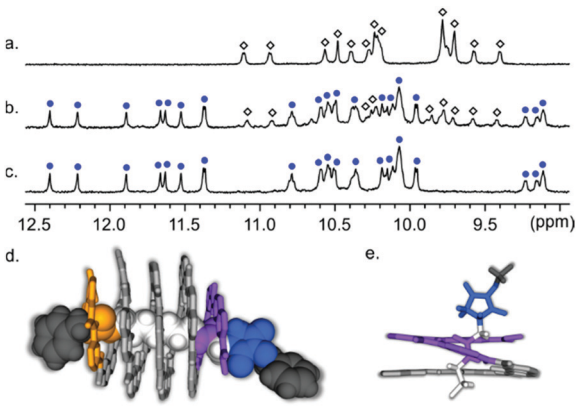

Fig. 2 Excerpts of the ^{1}H NMR spectra of **1** in $CDCl_3$ (300 MHz, 298 K, 1 mM) showing the amide resonances of: (a) **1** as a single helix and after the addition of (b) 1 equiv. and (c) 2 equiv. of axle **2**. Amide signals of single helix **1** and the foldaxane **1⊃2** are marked with diamonds and blue circles, respectively. (d) X-Ray structure of **1⊃2**. The axle is shown in CPK representation whereas the helix is shown either in tube. (e) Detailed views showing the binding mode in vicinity of the NHS group.

of diastereomeric complexes [*P*-**1**⊃(R)-**2**/*M*-**1**⊃(S)-**2**] and [*P*-**1**⊃(S)-**2**/*M*-**1**⊃(R)-**2**] in the same proportion (Fig. S6, ESI†). The absence of diastereoselectivity can be explained by the lack of interaction between helix **1** and the stereogenic centre of the NHS moiety. An apparent association constant K_a = 8500 M^{-1} was calculated by direct integration of the NMR resonances of **1** and **1⊃2**. Single crystals were obtained by slow diffusion of hexane in a chlorobenzene solution of **1⊃2** and the structure was refined in the orthorhombic *Pbca* space group (Fig. 2d–e). The disorder of the R and S axles in the crystalline structure could be modelled and confirmed the absence of diastereoselectivity as both can be indifferently found in either the *P* or *M* helix. The solid state structure also revealed that the space between the NHS moiety and **1** is kept to the minimum. Therefore, the DB24C8 is not given

the opportunity to reside between the NHS and the helix in the targeted foldarotaxane **1⊃3-Boc**.

We then attempted to predict the outcome of the wrapping of **1** around the fully functional [2]rotaxane **3-Boc** using molecular mechanics. For this purpose, the model of **1⊃3-Boc** was built using the Merck Molecular Force Field static (MMFFs) (Fig. 3f). Upon wrapping around the carbamate–amide station of **3-Boc**, the bulky helix **1** can displace the DB24C8 away from the amide station and compartmentalize the [2]rotaxane. The resulting foldarotaxane architecture combined both a rotaxane and a foldaxane arrangements. Because the "left" part of the axle is hindered by both the Boc group and **1**, the DB24C8 has sterically no other choice than shuttling across the NHS group and being compartmentalized on the "right" part of the axle despite the lack of any formal site of interactions for it. The supramolecular assembly of foldarotaxane **1⊃3-Boc** was then monitored by ^{1}H NMR (Fig. 3b–e). The formation of **1⊃3-Boc** indicates that the affinity between **1** and **3-Boc** is sufficiently large to overcome the interaction between the DB24C8 and the amide.¶ As for **1⊃2**, gradual addition of **3-Boc** on **1** in $CDCl_3$ led to the emergence of a new set of resonances in slow exchange on the NMR time scale. Saturation of helix **1** was reached after 144 hours using 2.5 equiv. of **3-Boc**. The slowness to reach the thermodynamic equilibrium is attributed to the presence of the bulky ends of the encircled axle, which prevent the helix from freely gliding over them. Additionally, over time, single helix **1** can dimerise back into parallel and anti-parallel double helix $(\mathbf{1})_2$ (Fig. 3a, left). To confirm the efficient foldamer-driven compartmentalization of **1⊃3-Boc**, cleavage of the foldarotaxane axle at its NHS ester reactive site was performed by adding 2.75 equiv. of the bulky 4, 4-diphenylbutylamine. The addition then elimination mechanism allowed for the preservation of the interlocked [2]rotaxane architecture because the DB24C8 was localized between the diphenyl stopper and the NHS ester. Indeed, at each stage of the mechanism, the ending groups were always large enough to ensure the mechanical bond. The aminolysis was followed by ^{1}H NMR monitoring of the amide region of **1⊃3-Boc** (Fig. 4b–e). The resonances of the foldarotaxane **1⊃3-Boc** progressively disappeared to be replaced by those of foldaxane **1⊃5u-Boc**. Reaction was complete after 18 h. Recycling GPC was used to remove the high molecular weight foldamer-containing species (*e.g.* **1⊃5u-Boc**, **1**) from the smaller components of the reaction. Further HPLC analysis on reverse phase was carried out and indicated the presence of the expected [2]rotaxane **6**. By-products **5u-Boc**, **6u** and DB24C8 were also detected: they resulted from the cleavage of the excess amount of rotaxane **3-Boc** used for the formation of the foldarotaxane **1⊃3-Boc**. Purification on silica gel chromatography allowed for the isolation of the improbable [2]rotaxane **6** in a 87% yield.

In summary, we reported herein the use of a foldamer helix to compartmentalize a [2]rotaxane molecular shuttle. Because of its greater affinity, helical foldamer **1** binds to axle of rotaxane **3-Boc** by displacing the macrocycle away from the amide. Models suggest, and covalent trapping experimentally confirms, that the macrocycle can only be located around the diphenylheptanoate part in **1⊃3-Boc**. To the best of our knowledge, this is the first utilisation of a foldamer helix as a supramolecular auxiliary in order to displace and sequestrate the surrounding macrocycle of a [2]rotaxane around a part of the encircled axle for which it has no formal site of interaction. This study opens the way to the design of novel molecular shuttles able to actuate through interdependent motion of foldamer and macrocycles along a same molecular axle. Well-designed foldamer-assisted molecular pump might also be envisaged.

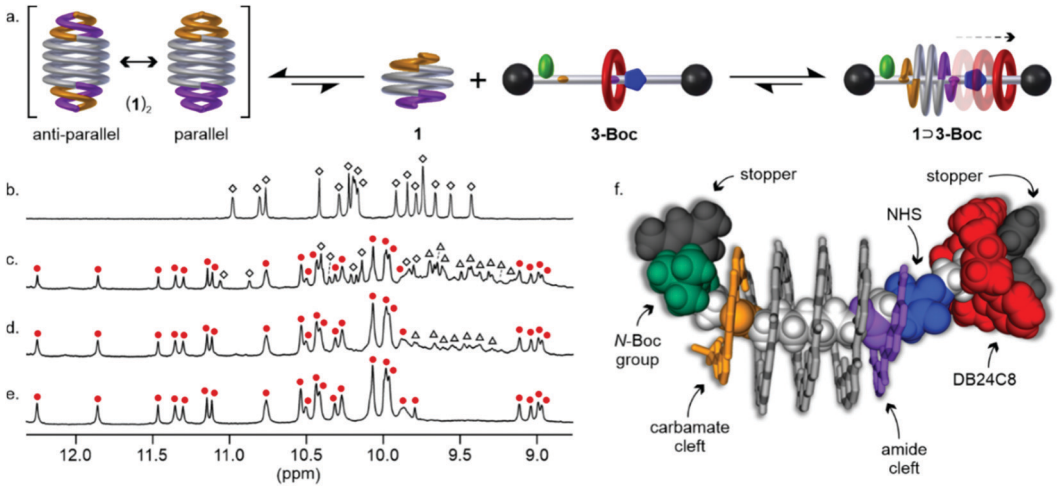

Fig. 3 (a) (*left*) Equilibrium between double helix $(\mathbf{1})_2$ and single helix **1**. Note that, as sequence **1** is dissymmetrical, $(\mathbf{1})_2$ can be either parallel or antiparallel. (*right*) The formation of the foldarotaxane **1⊃3-Boc** requires the unfolding and refolding of the helix around the molecular axle. The binding of **1** forces the translocation of the macrocycle (DB24C8) through the NHS moiety (blue pentagon). (b–e) Kinetic monitoring of the folding of single helix **1** (6 mM) around axle **3-Boc** (15 mM) in $CDCl_3$ followed by ^{1}H NMR (700 MHz, 298 K) and showing the amide resonances of the helix; (b) initial single helix **1**; (c) 18 h after the addition of **3-Boc**; then after (d) 72 h and (e) 144 h. For the equilibration procedure see the ESI.† Amide signals of **1**, $(\mathbf{1})_2$ and **1⊃3-Boc** are marked with diamonds, triangles and red circles, respectively. (f) Energy-minimized molecular model, built using MMFFs of the foldarotaxane **1⊃3-Boc**. The various functional groups are colour coded as in Fig. 1. Side chains and non-polar hydrogen atoms of the helix have been removed for clarity.

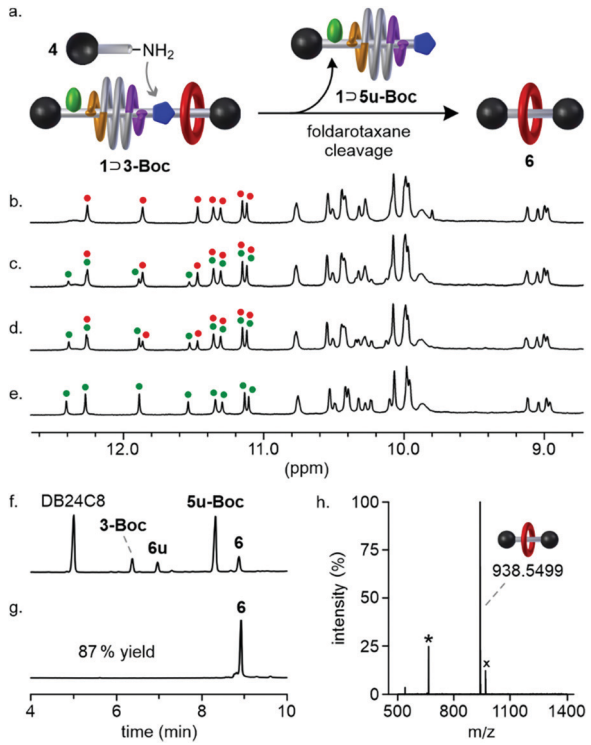

Fig. 4 (a) Cartoon illustrating the aminolysis of **1⊃3-Boc** that leads to rotaxane **6**. Parts of the ^{1}H NMR spectra (700 MHz, 298 K) showing the amide resonances of **1⊃3-Boc** (6 mM) in $CDCl_3$: (b) the initial **1⊃3-Boc** foldarotaxane; and in the presence of the amine **4** (16.5 mM) after: (c) 1 h, (d) 3 h 30 min and (e) 18 h. The resonances of **1⊃3-Boc** and **1⊃5u-Boc** are marked with red and green circles, respectively. HPLC chromatograms (C8 column, H_2O + 0.1% TFA/MeCN + 0.1% TFA −60 : 40 to 0 : 100, 293 K, 254 nm) of: (f) the mixture of the different components obtained after the aminolysis **1⊃3-Boc** at the exclusion of **1⊃5u-Boc** that has been previously removed by preparative GPC. (g) Rotaxane **6** after purification using silica chromatography. (h) Electrospray ionization mass spectrum (ESI-MS) of the rotaxane **6**. The star and the cross denoted an artefact of the mass spectrometer and an undetermined *m/z* value of [**6** + 28], respectively.

We thank the "Agence Nationale de la Recherche" for funding the project ANR-17-CE07-0014-01 and the France–Germany International Research Project "Foldamers Structures and Functions" (IRP FoldSFun). This work benefited from the facilities and expertise of the Biophysical and Structural Chemistry platform at IECB, CNRS UMS3033, INSERMUS001, and Bordeaux University, France.

Conflicts of interest

There are no conflicts to declare.

Notes and references

§ Improbable rotaxanes, also termed "impossible" rotaxanes in the literature, cannot be obtained through template-based synthetic methods because of the absence of formal mutual site of interaction. They are instead prepared using a mechanically interlocking auxiliary, or through active template or covalent-bond driven method, see ref. 13.
¶ It was not possible to determine a precise affinity constant for the complex as the NMR was too crowded to allow the correct integration of the different species resonances.

1 (*a*) S. Mena-Hernando and E. M. Pérez, *Chem. Soc. Rev.*, 2019, **48**, 5016; (*b*) A. Hashidzume, H. Yamaguchi and A. Harada, *Eur. J. Org. Chem.*, 2019, 3344.
2 (*a*) A. Credi, *Angew. Chem., Int. Ed.*, 2019, **58**, 4108; (*b*) C.-A. Cheng, T. Deng, F.-C. Lin, Y. Cai and J. I. Zink, *Theranostics*, 2019, **9**, 3341; (*c*) A. Fernandes, A. Viterisi, F. Coutrot, S. Potok, D. A. Leigh, V. Aucagne and S. Papot, *Angew. Chem., Int. Ed.*, 2009, **48**, 6443; (*d*) N. Pairault, R. Barat, I. Tranoy-Opalinski, B. Renoux, M. Thomas and S. Papot, *C. R. Chim.*, 2016, **19**, 103.
3 C. J. Bruns and J. F. Stoddart in *The nature of the mechanical bond: From Molecules to Machines*, Wiley, Hoboken, NJ, 2017.
4 (*a*) H. Tian and Q.-C. Wang, *Chem. Soc. Rev.*, 2006, **35**, 361; (*b*) S. Silvi, M. Venturi and A. Credi, *J. Mater. Chem.*, 2009, **19**, 2279; (*c*) S. Erbas-Cakmak, D. A. Leigh, C. T. McTernan and A. L. Nussbaumer, *Chem. Rev.*, 2015, **115**, 10081; (*d*) H.-Y. Zhou, Y. Han and C.-F. Chen, *Mater. Chem. Front.*, 2020, **4**, 12; (*e*) S. Kassem, T. van Leeuwen, A. S. Lubbe, M. R. Wilson, B. L. Feringa and D. A. Leigh, *Chem. Soc. Rev.*, 2017, **46**, 2592.
5 I. Aprahamian, *ACS Cent. Sci.*, 2020, **6**, 347.
6 For redox reaction, see: (*a*) R. A. Bissell, E. Córdova, A. E. Kalfer and J. F. Stoddart, *Nature*, 1994, **369**, 133for acid-base reaction, see: (*b*) W. L. Mock and J. A. Pierpont, *J. Chem. Soc., Chem. Commun.*, 1990, 1509for invertible covalent reactions, see: (*c*) J. Cao, M. C. T. Fyfe, J. F. Stoddart, G. R. L. Cousins and P. T. Glink, *J. Org. Chem.*, 2000, **65**, 1937; (*d*) H. Kawai, T. Umehara, K. Fujiwara, T. Tsuji and T. Suzuki, *Angew. Chem., Int. Ed.*, 2006, **45**, 4281; (*e*) D. A. Leigh and E. M. Pérez, *Chem. Commun.*, 2004, 2262.
7 (*a*) A. Altieri, G. Bottari, F. Dehez, D. A. Leigh, J. K. Y. Wong and F. Zerbetto, *Angew. Chem., Int. Ed.*, 2003, **42**, 2296; (*b*) J. J. Yu, *et al.*, *J. Org. Chem.*, 2019, **84**, 5790; (*c*) T. Kumpulainen, M. R. Panman, B. H. Bakker, M. Hilbers, S. Woutersen and A. M. Brouwer, *J. Am. Chem. Soc.*, 2019, **141**, 19118.
8 (*a*) D. A. Leigh, *et al.*, *Angew. Chem., Int. Ed.*, 2005, **44**, 3062–3067; (*b*) C. Romuald, A. Ardá, C. Clavel, J. Jiménez-Barbero and F. Coutrot, *Chem. Sci.*, 1851, **2012**, 3; (*c*) H. Tian, R. Li, P.-H. Lin and K. Meguellati, *New J. Chem.*, 2020, **44**, 10628.
9 (*a*) E. Busseron, C. Romuald and F. Coutrot, *Chem. – Eur. J.*, 2010, **16**, 10062; (*b*) D. Inamori, H. Masai, T. Tamaki and J. Terao, *Chem. – Eur. J.*, 2020, **26**, 3385.
10 (*a*) M. C. Jimenez-Molero, C. Dietrich-Buchecker and J.-P. Sauvage, *Chem. – Eur. J.*, 2002, **8**, 1456; (*b*) A. Caballero, L. Swan, F. Zapata and P. D. Beer, *Angew. Chem., Int. Ed.*, 2014, **53**, 11854; (*c*) T. A. Barendt, L. Ferreira, I. Marques, V. Felix and P. D. Beer, *J. Am. Chem. Soc.*, 2017, **139**, 9026; (*d*) R. C. Knighton and P. D. Beer, *Chem. Commun.*, 2014, **50**, 1540.
11 (*a*) A. Martinez-Cuezva, J. Berna, R.-A. Orenes, A. Pastor and M. Alajarin, *Angew. Chem., Int. Ed.*, 2014, **53**, 6762; (*b*) M. Calles, J. Puigcerver, D. A. Alonso, M. Alajarin, A. Martinez-Cuezva and J. Berna, *Chem. Sci.*, 2020, **11**, 3629.
12 M. Gauthier, V. Koehler, C. Clavel, B. Kauffmann, I. Huc, Y. Ferrand and F. Coutrot, *Angew. Chem., Int. Ed.*, 2021, **60**, 8380.
13 (*a*) J. S. Hannam, S. M. Lacy, D. A. Leigh, C. G. Saiz, A. M. Z. Slawin and S. G. Stitchell, *Angew. Chem., Int. Ed.*, 2004, **43**, 3260; (*b*) B. Riss-Yaw, C. Clavel, P. Laurent, P. Waelès and F. Coutrot, *Chem. – Eur. J.*, 2018, **24**, 13659; (*c*) P. Waelès, C. Clavel, K. Fournel-Marotte and F. Coutrot, *Chem. Sci.*, 2015, **6**, 4828; (*d*) S. Chao, C. Romuald, K. Fournel-Marotte, C. Clavel and F. Coutrot, *Angew. Chem., Int. Ed.*, 2014, **53**, 6914; (*e*) V. Aucagne, K. D. Hänni, D. A. Leigh, P. J. Lusby and D. B. Walker, *J. Am. Chem. Soc.*, 2006, **128**, 2186; (*f*) G. De, Bo, G. Dolphijn, C. T. McTernan and D. A. Leigh, *J. Am. Chem. Soc.*, 2017, **139**, 8455; (*g*) G. Schill and H. Zollenkopf, *Liebigs Ann. Chem.*, 1969, **721**, 53.
14 A. G. Kolchinski, D. H. Busch and N. W. Alcock, *J. Chem. Soc., Chem. Commun.*, 1995, 1289.
15 B. Riss-Yaw, J. Morin, C. Clavel and F. Coutrot, *Molecules*, 2017, **22**, 2017.
16 X. Wang, Q. Gan, B. Wicher, Y. Ferrand and I. Huc, *Angew. Chem.*, 2019, **131**, 4249.
17 (*a*) V. Koehler, A. Roy, I. Huc and Y. Ferrand, *Acc. Chem. Res.*, 2022, **55**, 1074; (*b*) Q. Gan, Y. Ferrand, C. Bao, B. Kauffmann, A. Grélard, H. Jiang and I. Huc, *Science*, 2011, **331**, 1172; (*c*) Y. Ferrand, Q. Gan, B. Kauffmann, H. Jiang and I. Huc, *Angew. Chem., Int. Ed.*, 2011, **50**, 7572; (*d*) Q. Gan, X. Wang, B. Kauffmann, F. Rosu, Y. Ferrand and I. Huc, *Nat. Nanotechnol.*, 2017, **12**, 447.